Journal of Solid State Chemistry 185 (2012) 143–149

Contents lists available at SciVerse ScienceDirect

Journal of Solid State Chemistry

journal homepage: www.elsevier.com/locate/jssc

Thermodynamic restrictions on mechanosynthesis of strontium titanate

J.F. Monteiro [a], A.A.L. Ferreira [b], I. Antunes [a], D.P. Fagg [c,*], J.R. Frade [a]

[a] Department of Ceramics and Glass Engineering, CICECO, University of Aveiro, 3810-193 Aveiro, Portugal
[b] Instituto Politécnico de Viana do Castelo, 4900-347 Viana do Castelo, Portugal
[c] Centro de Tecnologia Mecânica e Automação, Departamento de Engenharia Mecânica, Universidade de Aveiro, 3810-193 Aveiro, Portugal

ARTICLE INFO

Article history:
Received 24 June 2011
Received in revised form
18 October 2011
Accepted 29 October 2011
Available online 7 November 2011

Keywords:
Mechanochemistry
Mechanosynthesis
Strontium titanate
Chemical potential phase stability diagrams

ABSTRACT

Chemical potential phase stability diagrams were calculated from relevant thermodynamic properties and used to predict the thermodynamic driving force under prospective conditions of room temperature mechanosynthesis. One analysed the dependence of chemical potential diagrams on temperature and partial pressure of evolving gases such as oxygen or carbon dioxide, as expected on using strontium peroxide or strontium carbonate as precursor reactants for the alkali earth component. Thermodynamic calculations were also obtained for changes in titania precursor reactants, including thermodynamic predictions for reactivity of strontium carbonate with amorphous titania. Experimental evidence showed that strontium titanate can be obtained by mechanosynthesis of strontium carbonate + anatase mixtures, due to previous amorphization under high energy milling. Ability to perform mechanosynthesis with less energetic milling depends on the suitable choice of alternative precursor reactants, which meet the thermodynamic requirements without previous amorphization; this was demonstrated by mechanosynthesis from anatase + strontium peroxide mixtures.

1. Introduction

Repeated calcinations and re-grindings are often used to improve the quality of powders obtained by solid state reaction. Normally, this only yields milling to finer grain sizes, with additional improvement in overall homogeneity, without contribution to the formation of the intended resultant phase. However, high energy milling may also offer effective room temperature mechanosynthesis or mechanical alloying. Alkali earth precursor oxides are commonly obtained by previous thermal decomposition [1–4], and usually combined with anatase [1,5] to obtain corresponding titanates. Although one may find reports of mechanosynthesis of alkali earth titanates from mixtures of titania and hydroxides, there is convincing experimental evidence that TiO_2 + alkali earth oxide mixtures yield faster elimination of reactants and conversion to alkali earth titanates [3,6]. Direct room temperature mechanosynthesis was reported also for cases when the alkali earth precursor was barium peroxide BaO_2 [7]. Note that barium oxide reacts readily with atmospheric gases, causing the onset of barium carbonate or barium hydroxide [8]. Lead titanate or related perovskites also form readily by mechanosynthesis of $PbO + TiO_2$ powder mixtures [9,10], without risks of unwanted reactions of lead oxide with atmospheric humidity or CO_2.

As prepared alkali earth titanate powders obtained by mechanosynthesis often show poor crystallinity [5], even after several hours of milling, and XRD analyses show the co-existence of reactants with the reaction product. Nonetheless, incompletely reacted powders show ready conversion to crystalline titanates on heating to relatively low temperature, i.e., milling combines the onset of room temperature mechanosynthesis with efficient mechanical activation, which enhances faster conversion on heating [11].

Some attempts to use high energy milling to obtain titanates from corresponding $TiO_2 + ACO_3$ powder mixtures (A = Mg, Ca, Sr, Ba) are expected to act mainly as mechanical activation processes rather than true room temperature mechanosynthesis [12–18]. However, other authors have ascribed peaks in X-Ray diffractograms of mechanically activated $TiO_2 + CaCO_3$ mixtures to the onset of calcium titanate [6,19]; this seems rather surprising if one considers the stability of alkali earth carbonates at room temperature, and justifies a detailed examination of thermodynamic restrictions on mechanosynthesis.

Strontium titanate is certainly one of the most interesting study cases due to its wide range of demonstrated or prospective applications. Strong microstructural effects on properties also justify attempts to use different processing routes, including mechanosynthesis [2] or mechanical activation [11], usually after previous thermal decomposition of strontium carbonate.

* Corresponding author. Fax: +351 234 425 300.
E-mail address: duncan@ua.pt (D.P. Fagg).

0022-4596/$ - see front matter © 2011 Elsevier Inc. All rights reserved.
doi:10.1016/j.jssc.2011.10.044

Mechanosynthesis has also been reported for other members of the $Sr_{n+1}Ti_nO_{3n+1}$ series [7,20,21], using titania and strontium oxide precursors. In contrast, $Sr(OH)2\cdot 8H_2O$ was ill suited for direct mechanosynthesis [20], even when this alkali earth hydroxide was combined with more reactive titania precursors (e.g. tetrabutyl titanate [11]).

2. Elaboration of chemical potential diagrams

Evidence of room temperature mechanosynthesis from titania and strontium oxide [2] powders may suggest a relatively simple overall reaction

$$SrO + TiO_2 \rightarrow SrTiO_3 \quad (1)$$

However, this is an oversimplification when one takes into account that several other members of the Ruddlesden–Popper (RP) series $Sr_{n+1}Ti_nO_{3n+1}$ may also be formed [20]. The ternary system TiO_2–SrO–CO_2 system may also be considered to obtain wider thermodynamic guidelines for mechanical activation from commonly used titania+carbonate precursors. Interactions of strontium titanate and several intermediate $Sr_{n+1}Ti_nO_{3n+1}$ phases ($n=1$, 2, 3) with CO_2 essentially depend on the activity of the alkali earth species, which does not remain strictly constant, even within the stability window of a single solid state phase. Thus, phase stability diagrams for ternary systems are usually presented in triangular representations. Yet, Yokokawa et al. [22,23] proposed alternative planar phase stability diagrams as a function of a relevant activity ratio. This was used to analyse redox equilibria for a variety of systems such as La–*M*–O with *M*=Ni, Co, and Fe. In the present work one assumes that oxide components remains redox stable under powder preparation conditions, thus allowing reference to a pseudo-ternary SrO–TiO_2–CO_2 system, rather than the complex quaternary system Sr–Ti–O–C.

For the SrO–TiO_2–CO_2 system one identifies the single oxide phases SrO and TiO_2, the carbonate phase ($SrCO_3$), and several titanate phases (Sr_2TiO_4, $Sr_3Ti_2O_7$, $Sr_4Ti_3O_{10}$, and $SrTiO_3$), interacting with a single reactive gas (CO_2) in the atmosphere. In this case, equilibrium diagrams for SrO–TiO_2–CO_2, at a given temperature, may be represented by plots of $\log(a_{SrO}/a_{TiO_2})$ vs $\log(pCO_2)$, and will include three types of reactions, corresponding to:

(i) equilibria depending on pCO_2 only (e.g. reaction 2 for SrO/$SrCO_3$ equilibrium);
(ii) equilibria exclusively dependent on the activity ratio a_{SrO}/a_{TiO_2} (e.g. reaction 3 for $SrTiO_3/Sr_4Ti_3O_{10}$);
(iii) equilibria corresponding to interdependence between the activity ratio and pCO_2 (e.g. reaction 4 for $SrTiO_3/SrCO_3$).

$$SrO(s) + CO_2 \leftrightarrow SrCO_3(s) \quad (2)$$

$$SrO + 7SrTiO_3(s) \leftrightarrow TiO_2 + 2Sr_4Ti_3O_{10}(s) \quad (3)$$

$$SrO + SrTiO_3(s) + 2CO_2 \leftrightarrow 2SrCO_3(s) + TiO_2 \quad (4)$$

For the case of reaction 2 one may take into account that the activity in a single component calcia phase is unity, thus yielding a very simple expression for the equilibrium constant and

$$RT\ln(pCO_2) = \Delta G_2 \quad (5)$$

For reaction 3, one expressed equilibrium with unit stoichiometric coefficients for both oxide components in order to obtain direct correspondence between the activity ratio and mass action constant; this yields

$$RT\ln(a_{SrO}/a_{TiO_2}) = \Delta G_3 \quad (6)$$

Finally, reaction 4 was also written with unit stoichiometric coefficients for both oxide components, to simplify the relation between activity ratio and partial pressure of the reacting gas, i.e.:

$$RT\ln(a_{SrO}/a_{TiO_2}) = -2RT\ln(pCO_2) + \Delta G_4 \quad (7)$$

Similar approaches were used to obtain the corresponding relations for other 2-phase equilibria in the system SrO–TiO_2–CO_2 (Table 1). A suitable database [24] was then used to extract thermodynamic properties required to compute the relevant Gibbs free energy changes for those reactions, and to obtain the dependence of chemical activity ratio on partial pressure of carbon dioxide (Fig. 1), with an alternative predictions for rutile, anatase, and amorphous titania. Indeed, more advanced *ab-initio*

Table 1
Two-phase equilibria in the SrO–TiO_2–CO_2 system.

2-phase equilibria	Reaction
TiO_2(s)/$SrTiO_3$(s)	$SrO + TiO_2(s) \leftrightarrow SrTiO_3(s)$ $\ln(a_{SrO}/a_{TiO_2}) = \Delta G_1/(RT)$; (with $a_{TiO_2}=1$)
SrO(s)/$SrCO_3$(s)	$SrO(s) + CO_2(g) \leftrightarrow SrCO_3(s)$ $\ln(pCO_2) = \Delta G_2/(RT)$
$SrTiO_3$(s)/$Sr_4Ti_3O_{10}$(s)	$SrO + 7SrTiO_3(s) \leftrightarrow 2Sr_4Ti_3O_{10}(s) + TiO_2$ $\ln(a_{SrO}/a_{TiO_2}) = \Delta G_3/(RT)$
$SrTiO_3$(s)/$SrCO_3$(s)	$SrO + SrTiO_3(s) + 2CO_2(g) \leftrightarrow TiO_2 + 2SrCO_3(s)$ $\ln(a_{SrO}/a_{TiO_2}) = -2\ln(pCO_2) + \Delta G_4/(RT)$
$Sr_4Ti_3O_{10}$(s)/$SrCO_3$(s)	$SrO + 1/3Sr_4Ti_3O_{10}(s) + 7/3CO_2(g) \leftrightarrow TiO_2 + 7/3SrCO_3(s)$ $\ln(a_{SrO}/a_{TiO_2}) = -7/3\ln(pCO_2) + \Delta G_5/(RT)$
$Sr_3Ti_2O_7$(s)/$SrCO_3$(s)	$SrO + 0.5Sr_3Ti_2O_7(s) + 2.5CO_2(g) \leftrightarrow TiO_2 + 2.5SrCO_3(s)$ $\ln(a_{SrO}/a_{TiO_2}) = -2.5\ln(pCO_2) + \Delta G_6/(RT)$
Sr_2TiO_7(s)/$SrCO_3$(s)	$SrO + Sr_2TiO_4(s) + 3CO_2(g) \leftrightarrow TiO_2 + 3SrCO_3(s)$ $\ln(a_{SrO}/a_{TiO_2}) = -3\ln(pCO_2) + \Delta G_7/(RT)$
TiO_2(s)/$SrCO_3$(s)	$SrO + CO_2(g) \leftrightarrow SrCO_3(s)$ $\ln(a_{SrO}/a_{TiO_2}) = -\ln(pCO_2) + \Delta G_8/(RT)$; (with $a_{TiO_2}=1$)
Sr_2TiO_4(s)/SrO(s)	$Sr_2TiO_4(s) \leftrightarrow TiO_2 + 2SrO(s)$ $\ln(a_{SrO}/a_{TiO_2}) = \Delta G_9/(RT)$; (with $a_{SrO}=1$)
$Sr_3Ti_2O_7$(s)/Sr_2TiO_4(s)	$SrO + 3Sr_3Ti_2O_7(s) \leftrightarrow TiO_2 + 5Sr_2TiO_4(s)$ $\ln(a_{SrO}/a_{TiO_2}) = \Delta G_{10}/(RT)$
$Sr_4Ti_3O_{10}$(s)/$Sr_3Ti_2O_7$(s)	$SrO + 5Sr_4Ti_3O_{10}(s) \leftrightarrow TiO_2 + 7Sr_3Ti_2O_7(s)$ $\ln(a_{SrO}/a_{TiO_2}) = \Delta G_{11}/(RT)$
$SrTiO_3$(s)/$Sr_4Ti_3O_{10}$(s)	$SrO + 7SrTiO_3(s) \leftrightarrow 2Sr_4Ti_3O_{10}(s) + TiO_2$ $\ln(a_{SrO}/a_{TiO_2}) = \Delta G_{12}/(RT)$

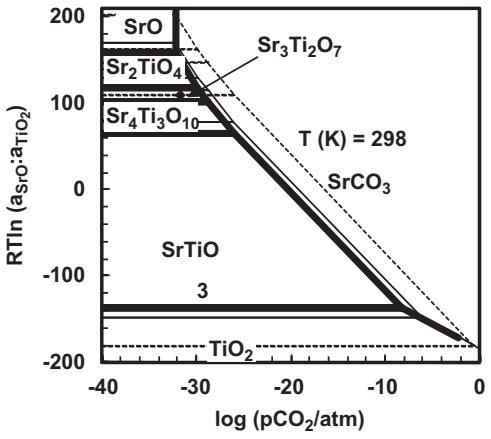

Fig. 1. Thermodynamic predictions of equilibrium diagram for the system TiO_2–SrO–CO_2 at 298 K. Thick lines were computed with thermodynamic properties of rutile, whereas thinner lines show the corresponding diagram for anatase, and the dashed lines for amorphous titania [28].

methods may be used to predict the reactivity of solids and decomposition reactions; this may be required for clarification of complex mechanisms (e.g. [25]), for fundamental studies of interactions of solids with atmospheric gases (e.g. [26]), to analyse tolerance of materials to contaminants (e.g. [27]), etc. However, *ab-initio* calculations are ill suited to show comprehensive correlations for multiphase systems, as exemplified in Fig. 1. In addition, *ab-initio* calculations are usually based on dedicated software packages and often require relatively long computing times. Our classical thermodynamic predictions can be based on a simple EXCEL spreadsheet (or similar widely available software), and calculation times are in the order of seconds.

3. Thermodynamic requirements for mechanosynthesis and mechanical activation.

The chemical potential diagram at room temperature (Fig. 1) predicts the co-existence of strontium titanate with rutile or anatase down to low values of partial pressure of carbon dioxide, i.e. far below typical contents of CO_2 in air (300–350 ppm). This emphasises that, from a thermodynamic perspective, one should not expect the formation of strontium titanate by mecanosynthesis of TiO_2+SrCO_3 powder mixtures in air, and that substitution of rutile by anatase would still be insufficient to meet the required thermodynamic conditions for room temperature synthesis. Nevertheless, thermodynamic calculations still suggest that room temperature mechanosynthesis may occur when using amorphous titania as a precursor. Note that the energy of amorphisation of anatase may be as high as 32 kJ/mol [28]. Indeed, the initial stages of mechanosynthesis or mechanical activation usually show gradual amorphisation of precursors, as revealed by XRD. However, these effects depend on the conditions of attrition, which may even cause transformation of anatase to the more stable polymorph (i.e. rutile) [29].

The predictions in Fig. 2 also provide a guideline of the thermodynamic driving force for reaction between titania and strontium carbonate, after mechanical activation. For example, the difference between two-phase equilibria for $SrCO_3/SrTiO_3$ and $SrTiO_3/TiO_2$ (Fig. 2), represent a combination of the overall chemical potential differences for the component oxides, i.e.:

$$RT\ln(a''_{SrO}/a''_{TiO_2})-RT\ln(a'_{SrO}/a'_{TiO_2})=RT\ln(a''_{SrO}/a'_{SrO})$$
$$-RT\ln(a''_{TiO_2}/a'_{TiO_2})=\Delta\mu_{SrO}-\Delta\mu_{TiO_2} \quad (8)$$

Thus, one may take these chemical potential differences as a thermodynamic driving force. Note that kinetic models for solid state reactions are usually related to one of these chemical potential differences [30,31]. For example, the kinetic constant for diffusion controlled formation of generic AB_2O_4 spinel with preferential transport of the divalent A^{2+} species and oxygen ions may be related to the chemical potential difference of the divalent oxide reactant, which corresponds to the Gibbs free energy change $\Delta\mu_{AO}=-\Delta G_R$ of the overall reaction $AO+B_2O_3\rightarrow AB_2O_4$ [30]. Similarly, one may take

$$\Delta\mu_{AO}=-\Delta G_R \quad (9)$$

For a typical reaction

$$ACO_3+TiO_2\rightarrow ATiO_3+CO_2 \quad (10)$$

where ΔG_R is the Gibbs free energy change of the overall reaction. In addition, local equilibrium in the perovskite phase implies $d\mu_{AO}=-d\mu_{BO_2}$ and thus:

$$0.5(\Delta\mu_{AO}-\Delta\mu_{BO_2})=0.5\Delta RT\ln(a_{AO}/a_{BO_2})=-\Delta G_R \quad (11)$$

This shows that chemical potential diagrams combine information on phase stability fields and also on the thermodynamic driving force for synthesis of individual phases. For example, the dashed line in Fig. 2 shows the chemical potential driving force for reaction between titania and strontium carbonate at 400 °C. Indeed, mechanical activation is still needed to overcome kinetic limitations, namely by yielding highly defective and nanostructured reactant particles.

Slow kinetics may also impose additional limitations on formation of titanate phases even after mechanical activation. For example, Hungria et al. [20] did not detect the formation of reaction products after heat treatment of mechanically activated $SrCO_3+TiO_2$ powders at 250 °C, for 12 h and only found traces of $SrTiO_3$ after calcinations at 600 °C, for 12 h. Note that the dependence on temperature probably combines Arrhenius-type activation and also a gradual increase in thermodynamic driving force, as shown in Fig. 2.

Fig. 3 compares the thermodynamic predictions for a CO_2 atmosphere and in nearly CO_2-free conditions, as expected for mechanosynthesis of TiO_2+SrO mixtures. Note that the initial atmospheric content of CO_2 in a closed reactor should be readily exhausted without significant formation of strontium carbonate, displacing the corresponding equilibrium conditions along the line $a\rightarrow a'$. Thus, one may assume that SrO effectively imposes CO_2-lean conditions and the thermodynamic conditions required for formation of strontium titanate at room temperature. Indeed,

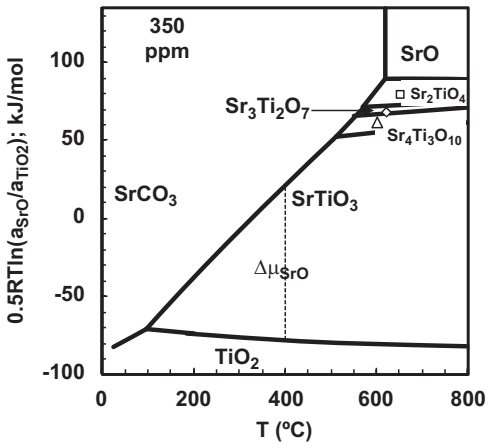

Fig. 2. Temperature dependence of chemical potential diagram for the TiO_2–SrO–CO_2 systems at 350 ppm of CO_2.

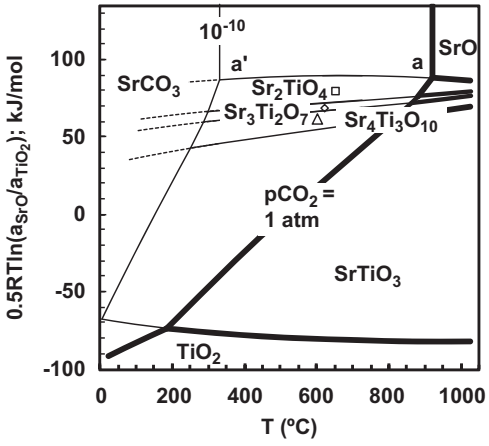

Fig. 3. Temperature dependence of chemical potential diagram for the TiO_2–SrO–CO_2 system, showing conditions for formation of strontium titanate and other intermediate phases (Sr_2TiO_4, $Sr_3Ti_2O_7$ and $Sr_4Ti_3O_{10}$) at $pCO_2=1$ atm (thick lines) and 10^{-10} atm (thin lines).

this buffer effect may be lost [8], after very long mechanical activation or if the reactor is opened to the ambient atmosphere.

Other results reported by Hungria et al. [20] for $SrCO_3$:TiO_2=3:2 are in close agreement with the chemical potential diagram shown in Fig. 3, namely the co-existence of $SrTiO_3$ and $SrCO_3$ for up to about 800 °C, and then complete reaction of strontium carbonate at $T \geq 900$ °C. Fig. 3 is also consistent with the transformation of $SrTiO_3$ to other $Sr_{n+1}Ti_nO_{3n+1}$ phases. The narrow chemical chemical potential difference across the domain of $Sr_3Ti_2O_7$ may explain the difficulties in preparation of this material as a single phase.

Peroxides are also possible precursors for alkali earth species. These precursors decompose to the corresponding oxides on heating at relatively low temperatures. Since very reducing conditions are needed to reduce alkali earth oxides to corresponding metals, or to reduce titania, one may assume that only the alkali earth peroxide undergoes oxygen losses as follows:

$$2SrO_2 \rightarrow 2SrO + O_2 \quad (12)$$

Thus, one may derive equilibrium diagrams for the corresponding TiO_2–SrO–O_2 system by considering the set of 2-phase equilibria shown in Table 2. The relevant thermodynamic data for SrO and SrO_2 can be found in Ref. [32], and were combined with previous information to obtain the relevant Gibbs free energy changes and the resulting chemical potential diagrams (Fig. 4). In this case, the chemical potential diagram predicts the onset of different titanate phases in contact with strontium peroxide, in the sequence $Sr_4Ti_3O_{10} \rightarrow Sr_3Ti_2O_7 \rightarrow Sr_2TiO_4$ as the atmosphere changes from pure O_2 towards slightly reducing conditions. However, the actual thermodynamic driving force for formation of $SrTiO_3$ is much higher than that of other $Sr_{n+1}Ti_nO_{3n+1}$ phases. Note also that the atmosphere is likely to remain close to pure oxygen, because this gas species evolves by the reaction between titania and strontium peroxide; further contributing to lower the driving force for the formation of secondary phases. In addition, mechanically assisted reactions are likely to progress after complete consumption of strontium peroxide, by reaction between intermediate $Sr_{n+1}Ti_nO_{3n+1}$ phases and residual titania, provided that the overall composition corresponds to the stoichiometric ratio Sr:Ti=1.

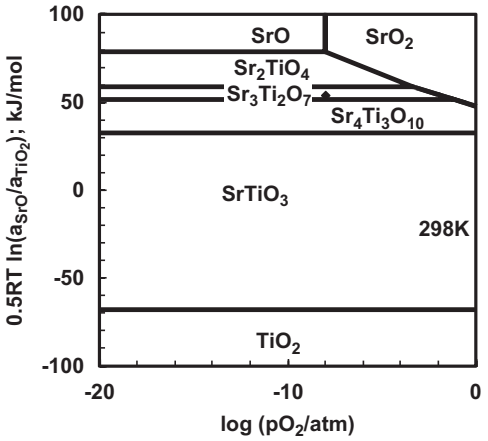

Fig. 4. Chemical potential diagrams describing conditions for synthesis of strontium titanate and other titanate phases (Sr_2TiO_4, $Sr_3Ti_2O_7$ and $Sr_4Ti_3O_{10}$) from TiO_2+SrO_2 at room temperature and versus oxygen partial pressure.

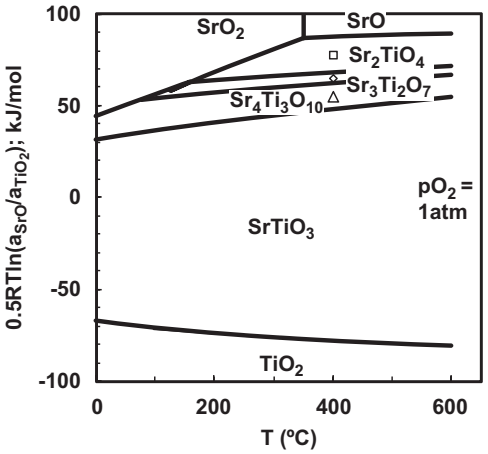

Fig. 5. Temperature dependence of chemical potential diagram for synthesis of strontium titanate and other intermediate phases (Sr_2TiO_4, $Sr_3Ti_2O_7$ and $Sr_4Ti_3O_{10}$) from TiO_2–SrO_2 in oxygen atmosphere (pO_2=1 atm).

Table 2
Two-phase equilibria in the SrO–TiO_2–O_2 system.

2-phase equilibria	Reaction
$SrO(s)/SrO_2(s)$	$2SrO(s)+O_2(g) \leftrightarrow 2SrO_2(s)$ $\ln(pO_2) = \Delta G/(RT)$
$Sr_2TiO_4(s)/SrO_2(s)$	$SrO+Sr_2TiO_4(s)+1.5O_2(g) \leftrightarrow TiO_2+3SrO_2(s)$ $\ln(a_{SrO}/a_{TiO_2}) = -1.5\ln(pO_2)+\Delta G/(RT)$
$Sr_3Ti_2O_7(s)/SrO_2(s)$	$SrO+0.5Sr_3Ti_2O_7(s)+1.25O_2(g) \leftrightarrow TiO_2+2.5SrO_2(s)$ $\ln(a_{SrO}/a_{TiO_2}) = -1.25\ln(pO_2)+\Delta G/(RT)$
$Sr_4Ti_3O_{10}(s)/SrO_2(s)$	$SrO+1/3Sr_4Ti_3O_{10}(s)+7/6O_2(g) \leftrightarrow TiO_2+7/3SrO_2(s)$ $\ln(a_{SrO}/a_{TiO_2}) = -7/6\ln(pO_2)+\Delta G/(RT)$
$SrTiO_3(s)/SrO_2(s)$	$SrO+SrTiO_3(s)+O_2(g) \leftrightarrow TiO_2+2SrO_2(s)$ $\ln(a_{SrO}/a_{TiO_2}) = -\ln(pO_2)+\Delta G/(RT)$
$TiO_2(s)/SrO_2(s)$	$SrO+1/2O_2(g) \leftrightarrow SrO_2(s)$ $\ln(a_{SrO}/a_{TiO_2}) = -1/2\ln(pO_2)+\Delta G/(RT)$; (with $a_{TiO_2}=1$)
$Sr_2TiO_4(s)/SrO(s)$	$Sr_2TiO_4(s) \leftrightarrow TiO_2+2SrO(s)$ $\ln(a_{SrO}/a_{TiO_2}) = \Delta G/(RT)$; (with $a_{SrO}=1$)
$Sr_3Ti_2O_7(s)/Sr_2TiO_4(s)$	$SrO+3Sr_3Ti_2O_7(s) \leftrightarrow TiO_2+5Sr_2TiO_4(s)$ $\ln(a_{SrO}/a_{TiO_2}) = \Delta G/(RT)$
$Sr_4Ti_3O_{10}(s)/Sr_3Ti_2O_7(s)$	$SrO+5Sr_4Ti_3O_{10}(s) \leftrightarrow TiO_2+7Sr_3Ti_2O_7(s)$ $\ln(a_{SrO}/a_{TiO_2}) = \Delta G/(RT)$
$SrTiO_3(s)/Sr_4Ti_3O_{10}(s)$	$SrO+7SrTiO_3(s) \leftrightarrow 2Sr_4Ti_3O_{10}(s)+TiO_2$ $\ln(a_{SrO}/a_{TiO_2}) = \Delta G/(RT)$
$TiO_2(s)/SrTiO_3(s)$	$SrO+TiO_2(s) \leftrightarrow SrTiO_3(s)$ $\ln(a_{SrO}/a_{TiO_2}) = \Delta G/(RT)$; (with $a_{TiO_2}=1$)

The evolution of chemical potential diagrams with increasing temperature is shown in Fig. 5, for pO_2=1 atm. This confirms thermodynamic conditions for the onset of intermediate secondary phases by reaction between titania and strontium peroxide or strontium oxide. Nevertheless, kinetics are also likely to promote ready reaction of intermediate titanate phases with residual titania, except possibly for cases when the overall composition deviates significantly from the intended stoichiometric ratio.

4. Experimental procedure and results

TiO_2+$SrCO_3$ or TiO_2+SrO_2 were used as alternative precursors for mechanosynthesis of $SrTiO_3$, using anatase (Aldrich, 99.8% purity) combined with the corresponding stoichiometric quantities of strontium carbonate (Aldrich, 99.9% purity), or strontium peroxide (Aldrich). Strontium peroxide was found to contain slight fractions of carbonate or hydroxide, which were determined by thermogravimetry, using the SETARAM TG-DTA/DSC Labsys Instrument. Donor-doped compositions $SrTi_{1-x}Nb_xO_3$ were also prepared from powder mixtures of anatase, strontium

peroxide, and Nb_2O_5 to assess changes in $a_{SrO} : a_{TiO_2}$ activity ratio [33]. Mechanosynthesis or mechanical activation was performed in a planetary ball mill (Retsch PM200) at 650 rpm or 350 rpm, with tetragonal zirconia balls (Tosoh Co.) and in a zirconia vial (Retsch). Powder:balls weight ratio was fixed at 1:10, and milling was performed by a series of 5 min steps with 5 min interruptions for cooling and to reverse direction of rotation after each interruption. Phase identification was performed by powder X-Ray diffraction with a Rigaku Geigerflex D/Max B diffractometer using Cu$K\alpha$ radiation (over the range $20^\circ \le 2\theta \le 70^\circ$ with a stepwidth of 0.02° and a scan rate of 3°/min). The presence of residual reactants (i.e. $SrCO_3$ or SrO_2) after mechanical activation or mechanosynthesis was monitored by thermogravimetry on heating at 5 °C/min, in air.

Fig. 6 confirms the ready formation of strontium titanate from a TiO_2+SrO_2 mixture milled at 650 rpm, thus confirming thermodynamic predictions that strontium peroxide is an efficient alkali earth precursor. In fact, the onset of strontium titanate is already obvious after 1 h, most probably combining the high thermodynamic driving-force with the ready amorphization of the precursor powders. The intensities of main XRD peaks of strontium titanate still increase even after flattening of precursor peaks, which suggests increased crystallinity of the titanate phase and/or further reaction of amorphous precursors.

The chemical potential diagram (Fig. 5) suggests the formation of $Sr_4Ti_3O_{10}$ at room temperature (Fig. 5). Thus, one cannot exclude the co-existence of this phase with strontium titanate, mainly because the main (110) peak of $SrTiO_3$ is distinctly asymmetric and too broad to be distinguished from corresponding reflections of RP phases such as $Sr_4Ti_3O_{10}$ and/or $Sr_3Ti_2O_7$. Note also that co-existence of $SrTiO_3$ and $Sr_3Ti_2O_7$ was found on heating mechanically activated TiO_2+SrCO_3 powder mixtures at intermediate temperatures [20].

Anatase and strontium peroxides are also suitable precursors for the main components of $SrTiO_3$-based materials with slight composition changes, as found for the nominal composition $SrTi_{0.95}Nb_{0.05}O_3$ (Fig. 7) milled at 650 rpm. In this case, partial substitution of Nb^{5+} by Ti^{4+} may cause significant changes in $a_{SrO} : a_{TiO_2}$ activity ratio, as revealed by onset of SrO-rich precipitates and, thus, *A*-site deficiency [33]. For preferential charge

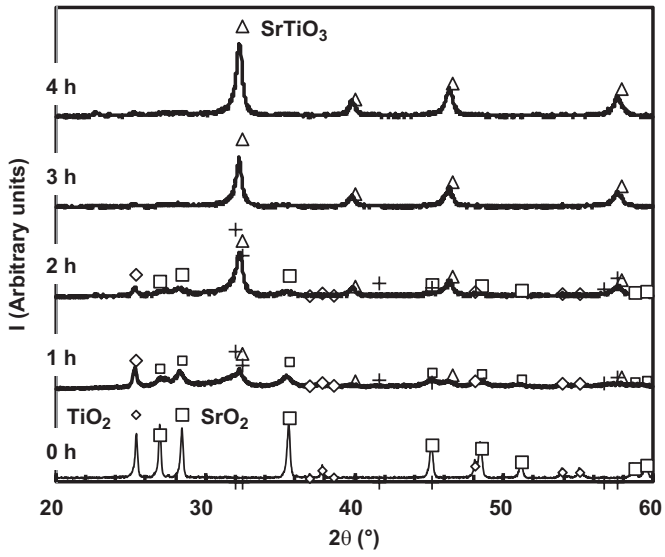

Fig. 6. X-Ray diffractograms of the starting TiO_2+SrO_2 mixture and after mechanical milling at 650 rpm, for 1, 2, 3, and 4 h. Different symbols are used to identify reflections ascribed to anatase (diamonds), SrO_2 (squares), and $SrTiO_3$ (triangles). The main reflection of $Sr_4Ti_3O_{10}$ (crosses) are shown to emphasise possible traces of this intermediate phase.

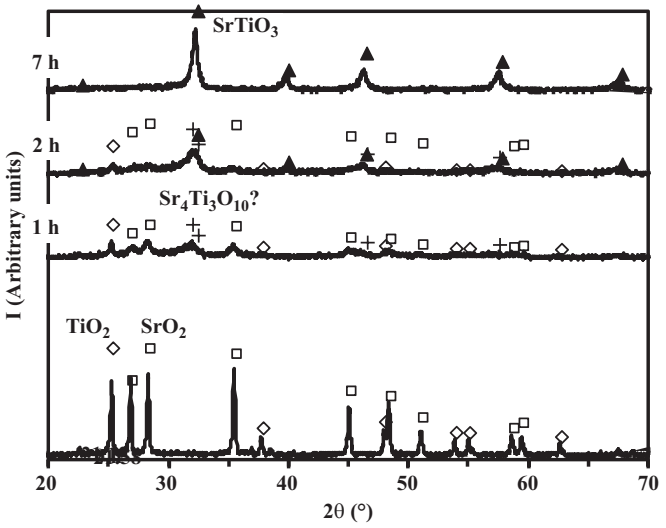

Fig. 7. X-Ray diffractograms of the starting $TiO_2+SrO_2+Nb_2O_5$ mixture and after mechanical milling at 650 rpm, for 1, 2, and 7 h. Different symbols are used to identify peaks ascribed to anatase (diamond), SrO_2 (square), Nb-doped $SrTiO_3$ (triangle), and possibly also traces of intermediate phase $Sr_4Ti_3O_{10}$ (crosses).

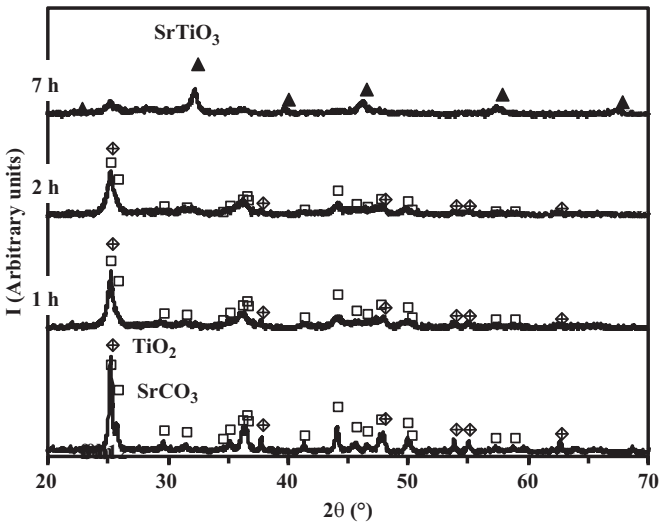

Fig. 8. X-Ray diffractograms of the starting TiO_2 (anatase)$+SrCO_3$ mixture and after mechanical milling at 650 rpm, for 1, 2, and 7 h. Different symbols are used to identify reflections ascribed to anatase (diamonds), $SrCO_3$ (squares) and $SrTiO_3$ (triangles).

compensation by *A*-site vacancies, as expected in air, one may assume that the SrO-rich precipitates correspond to RP-type phases, as follows:

$$SrO+(1-y)TiO_2+0.5yNb_2O_5 \rightarrow (1-0.5)Sr_{Sr}^{x}+0.5V_{Sr}''+(1-y)Nb_{Ti}^{\bullet}+yTi_{Ti}^{x}+3O_{O}^{x}+0.5SrO_{RP} \quad (13)$$

The chemical potential diagram for the TiO_2–SrO–CO_2 system (Fig. 1) suggests that direct room temperature mechanosynthesis of strontium titanate should not be possible on combining strontium carbonate with anatase or rutile. Thermodynamic inhibition is predicted for up to about 100 °C in contact with atmospheric CO_2 in air (300–350 ppm), and for up to about 200 °C in contact with a pure CO_2 atmosphere (Fig. 3). Nevertheless, the results in Fig. 8 show clear evidence that strontium titanate was obtained by mechanosynthesis of anatase+strontium carbonate mixtures at 650 rpm. Similarly, recent reports on mechanosynthesis of calcium titanate from anatase and calcium carbonate

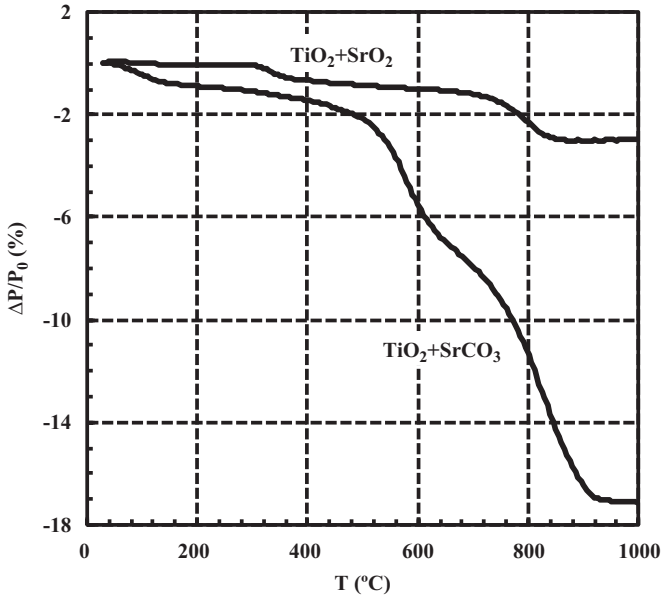

Fig. 9. Thermogravimetry of mechanically activated powders obtained from initial powder mixtures TiO_2+SrO_2 and TiO_2+SrCO_3, after milling for 7 h at 650 rpm.

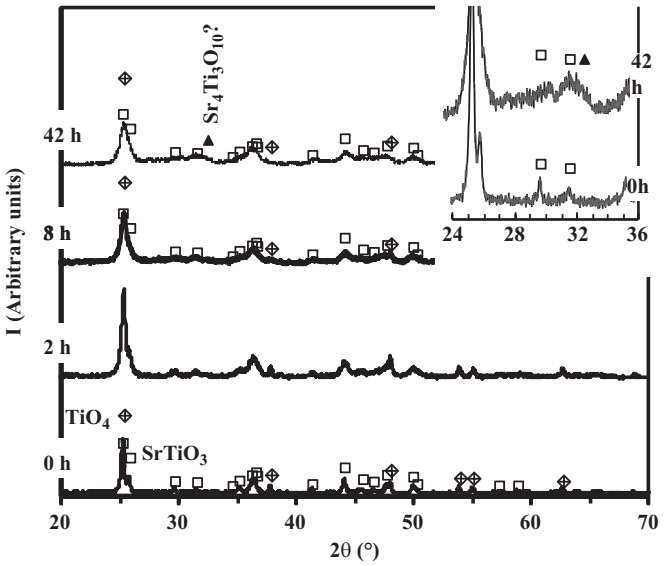

Fig. 10. XRD after mechanical milling of TiO_2 (anatase)+$SrCO_3$ powders at 350 rpm, for 0, 2, 8 and 42 h. Symbols denote peaks of $SrCO_3$ (squares), TiO_2 (diamonds) and filled triangles ($SrTiO_3$).

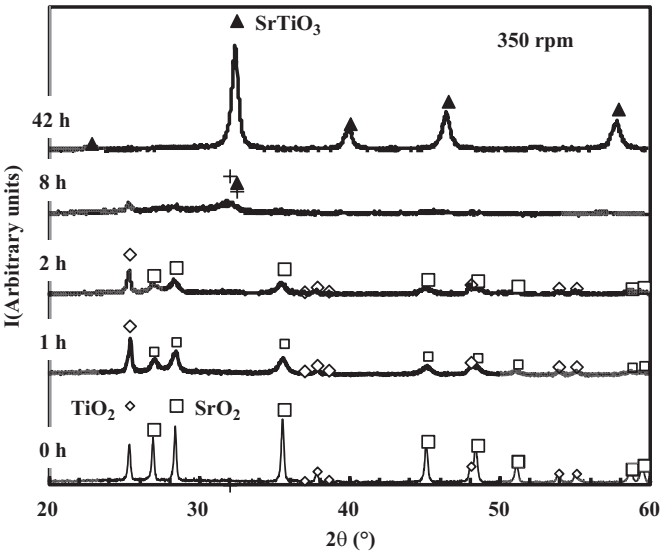

Fig. 11. XRD after mechanical milling of TiO_2 (anatase)+SrO_2 powders at 350 rpm, for 0, 2, 8 and 42 h. Symbols denote peaks of SrO_2 (squares), TiO_2 (diamonds) and filled triangles ($SrTiO_3$) and possibly also traces of intermediate phase $Sr_4Ti_3O_{10}$ (crosses).

[6,19] also contradict the predicted thermodynamic inhibition. Nevertheless, Figs. 1–3 may still provide explanations for this apparent contradiction, namely by taking into account that thermodynamic inhibition can be suppressed by amorphization. Indeed, the XRD results demonstrate that synthesis of reaction products is preceded by amorphisation (Fig. 8). This analogy is in agreement with the work of Steinike and Tkáčová [34] and also Boldyrev and Tkáčová [35], who suggest that the creation of mechanical activation induced defects leads to storage of energy in the solid, modifying the thermodynamic state. An alternative analogy is that relatively long milling times may lead to significant heating, especially if the experimental conditions correspond to a high ball to reactant ratio, and relatively long periods of milling before interruptions for cooling, as indicated in Ref. [6].

Thermogravimetry (Fig. 9) was used to confirm that a significant fraction of strontium carbonate converted during mechanical activation of TiO_2+SrCO_3 mixtures. In addition to initial losses at $T<150$ °C, possibly due to adsorbed humidity, one may distinguish different trends for typical ranges below and above about 620 °C. Indeed, decomposition of residual carbonate may be a complex process, as shown in Fig. 1, probably evolving from further formation of strontium titanate from amorphous reactants ($TiO_2+SrCO_3 \rightarrow SrTiO_3+CO_2$) to direct decomposition to strontium oxide ($SrCO_3 \rightarrow SrO+CO_2$) at the highest temperatures. The overall weight losses suggest that the residual carbonate content after mechanical activation is as high as ~82%, in a mostly amorphous form as found by XRD (Fig. 8).

Fig. 9 also shows incomplete reaction after mechanosynthesis from TiO_2+SrO_2 mixtures after 7 h of milling at 650 rpm. In this case, decomposition of residual reactants occurs in two main stages, suggesting decomposition of residual peroxide in the range 300–400 °C and then decomposition of strontium carbonate at 750–850 °C. Note that the starting peroxide reactant is far from phase pure, and contains a significant fraction of carbonate. From the actual weight losses one estimates about 81% conversion during the mechanosynthesis, with about 8% unreacted peroxide and 11% carbonate in the residual reactant fraction.

Amorphization of anatase+$SrCO_3$ mixtures is slower on lowering the rotation speed, and cannot be reached even after 42 h at 350 rpm (Fig. 10). Hence, this speed is insufficient to overcome the thermodynamic inhibitions. Note that there are still uncertainties concerning onset of traces of the titanate phase after 42 h, which is only suggested by a shoulder in the expanded insert shown in Fig. 10. The main difference between the results in Figs. 8 and 10 is, therefore, due to the ability of attaining sufficient amorphization of precursors. Less energetic milling was clearly insufficient to attain amorphization and failed to suppress the thermodynamic gap.

However, 350 rpm is still sufficient to promote mechanosynthesis from anatase+SrO_2 mixtures, as shown in Fig. 11. In this case, the reaction is thermodynamically favourable (Fig. 5), and the progress of reaction is mainly dependent on the ability to convey enough energy to overcome kinetic limitations. Note that the onset of strontium titanate is already obvious after 8 h of mechanical activation, and massive conversion to strontium titanate is found after 42 h.

5. Conclusions

Thermodynamic analysis can provide useful guidelines for prospects of mechanosynthesis at room temperature, or ready conversion of mechanically activated powder mixtures on heating to intermediate temperatures. Chemical potential diagrams were calculated to describe phase stability conditions, and to predict favourable conditions for room temperature synthesis. Although slight differences between the thermodynamic properties of different polymorphs may contribute to lower thermodynamic restrictions, this is unlikely to be sufficient to overcome those restrictions. Yet, this may be feasible for highly amorphous precursors, as predicted for the synthesis of strontium titanate from strontium carbonate and amorphous titania. In this case, high energy milling may contribute to meet thermodynamic conditions by previous amorphization of precursor reactants. Experimental confirmation was demonstrated by mechanosynthesis of strontium titanate from initial mixtures of strontium carbonate and anatase. This reaction is feasible under highly energetic milling and failed for less energetic milling. More efficient and faster mechanosynthesis was found when the starting precursor reactants ensure sufficient thermodynamic conditions, as demonstrated by mechanosynthesis of strontium titanate from mixtures of anatase + strontium peroxide. In this case, the main role of high energy milling is to enhance the kinetics of mechanosynthesis.

Acknowledgments

This work received funding from the European Union's Fund for Coal and Steel (RFCS) research program under grant agreement IERO-RSF-PR-09099 and was also partially supported by the FCT, Portugal.

References

[1] G. Mi, F. Sailo, S. Suzuki, Y. Waseda, Powder Technol. 97 (1998) 178–182 [5].
[2] N.J. Welham, J. Mater. Res. 13 (1998) 1607–1613.
[3] F.J. Berry, P. Wynn, J. Jiang, S. Morup, J. Mater. Sci. 36 (2001) 3637–3640.
[4] B.D. Stojanovic, A.Z. Simões, C.O. Paiva-Santos, C. Joyalekic, V.V. Mitic, J.A. Varela, J. Eur. Ceram. Soc. 25 (2005) 1985–1989.
[5] G. Mi, Y. Murakami, D. Shindo, F. Saito, Powder Technol. 105 (1999) 162–166.
[6] K.W. Ciurowa, P. Dulian, A. Nosal, J. Domagał, J. Therm. Anal. Calorim. 101 (2010) 471–477.
[7] T. Hungria, M. Alguero, A.B. Hungria, A. Castro, Chem. Mater. 17 (2005) 6205–6212.
[8] V.P. Pavlovi, D. Popovi, J. Krsti, J. Dojcilovi, B. Babi, V.B. Pavlovi, J. Alloys Compd. 486 (2009) 633–639.
[9] J. Xue, D. Wan, J. Wang, Mater. Lett. 39 (1999) 364–369.
[10] J.R.R. Siqueira, A.Z. Simoes, B.D. Stojanovic, C.O. Paiva-Santos, L.P.S. Santos, E. Longo, J.A. Varela, Ceram. Int. 33 (2007) 937–941.
[11] Q. Zhu, J.G. Xu, S. Xiang, L.X. Chen, Z.G. Tan, Mater. Lett. 65 (2011) 873–875.
[12] I.R. Evans, J.A.K. Howard, T. Sreckovic, M.M. Ristic, Mater. Res. Bull. 38 (2003) 1203–1213.
[13] V. Berbenni, A. Marini, J. Mater. Sci 39 (2004) 5279–5282.
[14] R.O. Fuentes, E. Chinarro, F.M. Figueiredo, R. Soares, F.M.B. Marques, J.R. Frade, J. Mater. Sci. 41 (2006) 7393–7400.
[15] O. Abe, Mater. Sci. Forum 225 (1996) 563–568.
[16] C. Gomez-Yanez, C. Benitez, H.B. Ramirez, Ceram. Int. 26 (2000) 271–277.
[17] V. Berbenni, A. Marini, G. Bruni, Thermochim. Acta 374 (2001) 151–158.
[18] J. Xue, J. Wang, D. Wan, J. Am. Ceram. Soc. 83 (2002) 232–234.
[19] S. Palaniandy, N.H. Jamil, J. Alloys Compd. 476 (2009) 894–902.
[20] T. Hungrıa, J.G. Lisoni, A. Castro, Mater. Chem. 14 (2002) 1747–1754.
[21] T. Hungria, I. MacLaren, H. Fuess, J. Galy, A. Castro, Mater. Lett. 62 (2008) 3095–3098.
[22] H. Yokokawa, N. Sakai, T. Kawada, M. Dokiya, J. Am. Ceram. Soc. 72 (1989) 2104–2110.
[23] H. Yokokawa, T. Kawada, M. Dokiya, J. Am. Ceram. Soc. 72 (1989) 133–152.
[24] C.W. Bale, A.D. Pelton, W.T. Thompson, G. Eriksson, K. Hack, P. Chartrand, S. Decterov, J. Melançon, S. Petersen, Factsage 5.5 chemical thermodynamic database, Thermfact and GTT-Technologies (1976-2007).
[25] D. Chakraborty, R.P. Muller, S. Dasgupta, W.A. Goddard, J. Phys. Chem. 104 (2000) 2261.
[26] G. Pacchioni, J.M. Ricart, F. Illas, J. Am. Chem. Soc. 116 (1994) 10152–10158.
[27] Y.M. Choi, C. Compson, M.C. Lin, M.L. Liu, J. Alloys Compd. 427 (2007) 25–29.
[28] H. Zhang, J.F. Banfiekld, Chem. Mater. 14 (2002) 4145–4154.
[29] S. Bégin-Colin, T. Gitot, G. le Caer, A. Mocellin, J. Solid State Chem. 149 (2000) 41–48.
[30] H. Schmalzried, Chemical Kinetics of Solids, Verlag, Weinheim, Germany, 1995, pp. 146–153.
[31] J.R. Frade, Solid State Ionics 101-103 (1997) 373–379.
[32] D. Risold, B. Hallstedt, L.J. Gauckler, Calphad 20 (1996) 353–361.
[33] J.C.C. Abrantes, J.A. Labrincha, J.R. Frade, Sensors and Actuators B 56 (1999) 198–207.
[34] U. Steinke, K. Tkáčová, J. Mater. Synth. Process. 8 (3-4) (2009) 197–203.
[35] V.V. Boldyrev, K. Tkáčová, J. Mater. Synth. Process. 8 (3–4) (2009) 121–132.